

# *H. sinensis* mycelium inhibits epithelial–mesenchymal transition by inactivating the midkine pathway in pulmonary fibrosis

Li Lu<sup>1</sup>, Haiyan Zhu<sup>1</sup>, Hailin Wang<sup>1</sup>, Huaping Liang (✉)<sup>3</sup>, Yayi Hou (✉)<sup>1,2,4</sup>, Huan Dou (✉)<sup>1,2,4</sup>

<sup>1</sup>The State Key Laboratory of Pharmaceutical Biotechnology, Division of Immunology, Medical School, Nanjing University, Nanjing 210093, China; <sup>2</sup>Department of Rheumatology and Immunology, Nanjing Drum Tower Hospital, The Affiliated Hospital of Nanjing University Medical School, Nanjing 210008, China; <sup>3</sup>State Key Laboratory of Trauma, Burns and Combined Injury, Research Institute of Surgery, Daping Hospital, The Army Medical University, Chongqing 400042, China; <sup>4</sup>Jiangsu Key Laboratory of Molecular Medicine, Nanjing University, Nanjing 210093, China

© Higher Education Press 2020

**Abstract** The medical fungus *Hirsutella sinensis* has been used as a Chinese folk health supplement because of its immunomodulatory properties. Our previous studies established the antifibrotic action of *Hirsutella sinensis* mycelium (HSM) in the lung. The epithelial–mesenchymal transition (EMT) is involved in the pathogenesis of idiopathic pulmonary fibrosis. The present study investigates the role of HSM in mediating EMT during the development of pulmonary fibrosis. HSM significantly inhibits bleomycin (BLM)-induced pulmonary fibrosis by blocking the EMT. In addition, the expression levels of midkine are increased in the lungs of the BLM-induced group. Further analysis of the results indicates that the mRNA level of midkine correlated positively with EMT. HSM markedly abrogates the transforming growth factor  $\beta$ -induced EMT-like phenotype and behavior *in vitro*. The activation of midkine related signaling pathway is ameliorated following HSM treatment, whereas this extract also caused an effective attenuation of the induction of EMT (caused by midkine overexpression) *in vitro*. Results further confirm that oral medication of HSM disrupted the midkine pathway *in vivo*. Overall, findings suggest that the midkine pathway and the regulation of the EMT may be considered novel candidate therapeutic targets for the antifibrotic effects caused by HSM.

**Keywords** epithelial–mesenchymal transition; *H. sinensis* mycelium; midkine; pulmonary fibrosis

## Introduction

Idiopathic pulmonary fibrosis (IPF) is an irreversible, progressive, and destructive disease accused by interstitial pneumonia that leads to excessive extracellular matrix deposition and death due to respiratory failure within five years from disease onset. This mortality incidence is noted among approximately 50% of the patients [1]. In recent years, the incidence of IPF has been gradually increased, and the median survival time following diagnosis is approximately below 2–3 years [2]. However, a limited number of effective clinical treatments have merely been used for IPF. The clinical application of Pirfenidone and

Nintedanib has certain side effects [3–5]. Pirfenidone induces hepatic dysfunction, gastrointestinal intolerance, and fatigue [6]. Nintedanib is an inhibitor of tyrosine kinase enzymes, which reduces proliferation, migration, and survival of fibroblasts. Moreover, the treatment of Nintedanib is not recommended among patients with moderate or severe liver disease [7,8]. Therefore, various studies have explored the design of alternative treatments for IPF.

Notably, *Cordyceps sinensis*, which is a Chinese herbal medicine, is a rare treatment regimen that is uniquely applied in China to treat parasitic life cycle. *Cordyceps sinensis* has been known in Asia as a popular folk remedy used for the treatment of various ailments, including cancer, liver disease, fatigue, renal dysfunction, and respiratory disease [9]. Previous studies have indicated that *Cordyceps sinensis* exhibited antitumor, anti-inflammatory, antioxidant, anti-infective, and antiaging activities [10]. However, a sharp decline has been noted in its annual

Received June 2, 2019; accepted November 27, 2019

Correspondence: Huan Dou, douhuan@nju.edu.cn;

Yayi Hou, yayihou@nju.edu.cn;

Huaping Liang, 13638356728@163.com

production, and a marked increase is evident in its commercial cost, thereby hindering the wide application of *Cordyceps sinensis* throughout Asia. Therefore, a mycelium extract of *Hirsutella sinensis* (HSM) was identified. Recent studies have demonstrated that the characteristics of HSM closely matched those of wild *Cordyceps sinensis* fruiting bodies in terms of culture conditions and biochemical composition [11,12]. Consequently, HSM became a valuable substitute for the production of *Cordyceps sinensis* [13–15]. Previous studies in our laboratory demonstrated the antifibrotic effects of HSM in bleomycin (BLM)-induced lung tissues, although the underlying mechanism remains unknown [16].

Activated fibroblasts and myofibroblasts have been proposed as the main effector cells that can secrete extracellular matrix proteins. Injured epithelial cells contribute to the formation of pulmonary fibrosis via the epithelial–mesenchymal transition (EMT), which is the process of transforming differentiated mature epithelial cells into mesenchymal cells by transforming growth factor- $\beta$ 1 (TGF- $\beta$ 1)-mediated stimulation [17–20]. Furthermore, certain studies have demonstrated that EMT was involved in abnormal epithelial–mesenchymal interactions that could repeatedly damage the alveolar epithelial cells and promote inflammation. The release of inflammatory factors that promote formation of fibrotic microenvironment can eventually lead to severe pulmonary fibrosis [21,22]. Therefore, the role of HSM in EMT during the development of pulmonary fibrosis should be investigated.

Midkine is a basic heparin-binding growth factor that promotes cell proliferation [23,24], differentiation [25,26], survival, and migration [27,28]. Furthermore, this growth factor is involved in a variety of biological processes, including neuronal development, angiogenesis, tumorigenesis, and inflammation [29,30]. Midkine has low expression level in tissues of normal adult mice. However, following damage of tissues, the expression levels of midkine were elevated in certain cell types such as the epidermal and bronchial epithelial cells [31]. Midkine exerted a specific role in organ fibrosis. High expression levels of midkine were detected in patients with acute respiratory distress syndrome (ARDS), which is a relatively common and lethal or disabling syndrome. Pulmonary fibrosis was significantly reduced in midkine<sup>-/-</sup> mice, which suggest a profibrotic effect of midkine. The profibrotic effect may be mediated via the NOX1-midkine-Notch2-angiotensin-converting enzyme (ACE) pathway [32,33]. Additional studies have demonstrated that midkine activated the EMT in pancreatic cancer and lung adenocarcinoma cells [34,35]. Moreover, previous studies have shown that midkine induced EMT via the activation of Notch2 signaling in human keratinocytes [36]. The aforementioned studies indicated that the overexpression

of midkine contributes to EMT and that the depletion of midkine induces the reversal of EMT to the mesenchymal–epithelial transition. A recent study on the role of midkine among IPF patients demonstrated that the serum midkine levels were significantly higher than those noted among healthy subjects, whereas midkine-deficient mice indicated low expression levels of collagen and  $\alpha$ -smooth muscle actin ( $\alpha$ -SMA), as well as reduced fibrotic symptoms [37]. Therefore, midkine should be involved in the development of pulmonary fibrosis by affecting the development of EMT.

HSM's regulation of EMT during the development of pulmonary fibrosis remains unknown. The present study aims to investigate the role of HSM in EMT and EMT-related pulmonary fibrosis *in vitro* and *in vivo*. Consequently, TGF- $\beta$ 1-induced EMT is repressed by treatment with HSM via the inactivation of the midkine signaling pathway.

## Materials and methods

### Preparation of HSM

HSM was originally obtained from Nanjing Zhongke Group (Nanjing, China). The detailed preparation of HSM was described in our previous study [16].

### Mouse model of pulmonary fibrosis

The present study was conducted in accordance with the institutional guidelines for the care and use of animals that were provided by the Nanjing University's Animal Care Commission. Male C57BL/6 mice (SCXK (SU) 2015-0001, Nanjing, China) without pathogens were obtained from the Model Animal Research Center of the Nanjing University and maintained under controlled conditions (indoor temperature of  $22 \pm 1^\circ\text{C}$  and 50%–60% humidity) at a 12-h dark/light cycle. The mice were fed with standard laboratory chow and water.

A total of 60 male C57BL/6 mice aged 7–8 weeks that weighed  $20 \pm 2$  g, were randomly divided into the following five experimental groups ( $n = 12/\text{group}$ ), namely, (1) normal control group, (2) BLM group, (3) BLM + HSM1 group (160 mg/kg/day), (4) BLM + HSM2 group (480 mg/kg/day), and (5) HSM group (480 mg/kg/day). The mice were injected by intratracheal instillation with 3 mg/kg of BLM (Haizhenghuirui, Serial Number: 17047411, China) via tracheostomy to induce pulmonary fibrosis. The mice in the control and HSM groups received an intratracheal administration of an equivalent volume of vehicle (saline). From day 5 to day 21 following the BLM instillation, the BLM + HSM and HSM groups received HSM in 500  $\mu\text{L}$  saline by intragastric administration every succeeding day.

Concomitantly, the mice in the control and BLM groups received an identical volume of saline. All the mice were sacrificed at the end of day 21 following BLM or saline treatment.

### Histopathology of lung tissues

The anterior and middle lobe of the right lungs were fixed in 10% neutral formalin for 48 hours, embedded in paraffin, and subsequently sectioned for hematoxylin and eosin (H&E) and Masson staining.

### Hydroxyproline assay

The left lobe lung samples were obtained from each group on the 21st day following the BLM treatment, and the lung collagen content was determined by analyzing hydroxyproline levels using the hydroxyproline assay kit (Jiancheng Inc., Nanjing, China) according to the instructions of the manufacturers.

### Immunostaining for tissues and cells

Ten percent buffered formalin-fixed and paraffin-embedded tissue blocks were cut into 5  $\mu\text{m}$ -thick sections. The sections were treated with a 0.1% hydrogen peroxide–methanol solution to inhibit endogenous peroxidase activity and were incubated with 5% bovine serum albumin (BSA) to block any nonspecific binding caused by primary antibodies. Subsequently, the sections were incubated with primary antibodies against anti- $\alpha$ -SMA (1:2000, Abcam, Cambridge, UK), anti-E-cadherin (1:2000, Proteintech, USA), and anti-midkine (5–15  $\mu\text{g}/\text{mL}$ , R&D Systems, USA) at 4 °C overnight. These sections were incubated with horseradish peroxidase (HRP)-conjugated polymer anti-rabbit or anti-mouse antibodies. The peroxidase activity was visualized using 0.1% 3,3'-diaminobenzidine and 0.01% hydrogen peroxide in Tris-buffered saline. Immunofluorescence assay was performed through the treatment of the sections with the primary antibodies against anti-vimentin (1:200, Proteintech, USA), anti- $\alpha$ -SMA (1:300, Sigma, USA), anti-N-cadherin (1:300, Proteintech, USA), anti-midkine (5  $\mu\text{g}/\text{mL}$ , R&D Systems, USA), and anti-Notch2 (1:400, Cell Signaling Technology, USA) at 4 °C overnight. These sections were incubated with secondary antibodies against goat anti-mouse IgG H&L (TRITC) (1:200, Abcam, Cambridge, UK) or Alexa Fluor® 488 AffiniPure Goat Anti-rabbit IgG (H + L) (1:200, FMS-RBaf48801, FcMACS, Nanjing, China), counterstained with DAPI (1:3000) for nuclear detection, and analyzed by immunofluorescence using the fluorescence microscope (Nikon 80i, Japan).

### Cell lines and cell culture

A549 cells were obtained from the Shanghai Institute of Cell Biology (Shanghai, China). The cells were grown in Dulbecco's Modified Eagle's medium (Gibco Inc., USA) with 10% heat-inactivated fetal bovine serum (Gibco Inc., USA) and 100 U/mL penicillin–streptomycin at 37 °C in a humidified atmosphere with 5%  $\text{CO}_2$ . Mouse primary type II AECs were obtained from Jiangsu Kejing Biotechnology (Jiangsu, China), and the purity was over 90% by detecting the marker pulmonary surfactant protein C (SP-C) (see Supplementary Material).

### Plasmid transfection

In the previous study conducted by our group, the pcDNA3.1/midkine plasmid was used [38]. A549 cells and mouse primary type II AECs were cultured to 80%–85% confluence and were pretreated with HSM for 2 hours. The cells were transfected by the DeofectEU Transfection Reagent (Baidai, Changzhou, China) and were collected 24 hours after transfection.

### CCK8 cell viability assay

A549 cells and mouse primary type II AECs ( $2 \times 10^4$  cells/well) were seeded in 96-well plates for cell viability assays. Following overnight culture, the cells were incubated with various concentrations of HSM (6.25, 12.5, 25, 50, 100, 200, 400, 800, 1600  $\mu\text{g}/\text{mL}$ ) for 24 hours. Subsequently, 10  $\mu\text{L}$  CCK8 (Dojindo, Japan) reagent was added to each cell and incubated for an additional 0.5–4 hours. The absorbance was measured at 450 nm using microplate reader (BioTek, Winooski, VT, USA).

### Fluorescence-based quantitative polymerase chain reaction (qRT-PCR)

Total ribonucleic acid (RNA) from A549 cells, mouse primary type II AECs, or frozen lung tissues were extracted by the TRIzol reagent (Invitrogen, USA) and reverse-transcribed by a reverse transcription kit (HiScript® II Q PT SuperMix for qPCR, Vazyme Biotech, Nanjing, China). Subsequently, the cDNAs were used as templates for the qRT-PCR analysis that is performed on the BIOER Line Gene 9640 detection system (Hangzhou, China). The Ct value and the relative expression levels of each gene were calculated according to the following formula  $2^{-\Delta\Delta\text{Ct}}$ . The relative amount of the target gene and the reference gene *GAPDH* were obtained. All the reactions were repeated thrice. All RNA samples exhibited a 260/280 ratio of  $\approx 2.0$ . Table 1 presents the primer sequences.

**Table 1** Primers used for q-PCR in this study

	Forward (5'–3')	Reverse (5'–3')
Midkine	CGCGTTCGCCAAAAAGAAAG	TACTTGCAGTCGGCTCCAAAC
h-NOX1	TTGTTGGTTAGGGCTGAATGT	GCCAATGTTGACCCAAGGATTTT
h-Notch2	CCTTCCACTGTGAGTGTCTGA	AGGTAGCATCATTCTGGCAGG
h-ACE	GGAGGAATATGACCGGACATCC	TGGTTGGCTATTGTCATGTTCTT
h-vimentin	GCCCTAGACGAACTGGGTC	GGCTGCAACTGCCTAATGAG
h-E-cadherin	CGAGAGCTACA-CGTTACCG	CGAGAGCTACACGTTACCG
h-GAPDH	AGAAGGCTGGGGCTCATTG	AGGGGCCATCCACAGTCTTC
h-N-cadherin	TTTGATGGAGGTCTCCTAACACC	ACGTTTAACACGTTGAAAATGTG
m-vimentin	CGTCCACACGCACCTACAG	GGGGGATGAGGAATAGAGGCT
m-E-cadherin	GTGCAGGTGTCCGATGTCAA	GGAGATTAACGAGGAGAGTGGC
m-N-cadherin	AGGCTTCTGGTGAAATTGCAT	GTCCACCTTGAAATCTGTGG
m-NOX1	GCTGGATTTGAGAGCGTTGC	GGTGGTATCTAGGGCTATGCT
m-Notch2	GAGAAAAACCGCTGTCAGAATGG	GGTGGAGTATTGGCAGTCCTC
m-ACE	ATGACAAGCGACTTCTCCCC	CCAAACCGAGGACCCCATAGA
m-GAPDH	AACGACCCCTTCATTGAC	TCCACGACATACTCAGCAC

### Western blot analysis

Lung tissues were homogenized in protein lysis buffer at 4 °C for 30 minutes. The buffer contained protease and phosphatases inhibitors. The samples were centrifuged (12 000 × *g*, 10 minutes at 4 °C), and the supernatants were collected. The protein concentrations levels were determined by the bicinchoninic acid protein assay kit (Beyotime Biotechnology, China). An equivalent of 60–90 µg of total protein was resolved on an 8%–12% SDS gel by PAGE. The proteins were transferred to polyvinylidene fluoride (PVDF) membranes (Millipore Co, Bedford, MA, USA). These membranes were blocked with 5% BSA for 2 hours at room temperature and subsequently treated with primary antibodies such as anti-vimentin (1:4000, Proteintech, USA), anti-N-cadherin (1:2000, Proteintech, USA), anti-E-cadherin (1:5000, Proteintech, USA), anti-NOX1 (1:1000, Proteintech, USA), anti-midkine (2 µg/mL, R&D Systems, USA), anti-Notch2 (1:1000, Cell Signaling Technology, USA), anti-ACE (1:1000, Proteintech, USA), and anti-GAPDH (1:1000, GOOD HERE, China) at 4 °C overnight. Afterward, the membranes were incubated with HRP-conjugated goat anti-rabbit IgG (1:4000, FCMACA, China), polyclonal sheep IgG (1 µg/mL, R&D Systems, USA) or rabbit anti-goat IgG (1:2000, Proteintech, USA) for 2 hours. An enhanced chemiluminescence kit (Supersignal™ West Pico PLUS, Thermo, USA) was utilized to detect the immunoreactive bands, and the densitometry analysis was performed by the Image J software (National Institutes of Health, Bethesda, MD, USA). GAPDH was used as the internal control.

### Statistical analysis

Data were expressed as mean ± SEM. Statistical analyses were performed by Graphpad Prism 5 (San Diego, CA, USA). Multigroup comparisons were analyzed by the student's *t*-test or the one-way ANOVA. A *P*-value less than 0.05 (*P* < 0.05) was considered for significant differences. The nonquantitative results were reported at least thrice.

## Results

### HSM attenuated lung fibrosis and EMT changes in BLM-treated mice

Fig. 1A illustrates the experimental plan. Our previous study demonstrated that HSM prophylactic administration (pre-administration of remodeling) relieved pulmonary fibrosis [16], thereby prompting us to explore the effectiveness of the therapeutic administration (administered following modeling). Another difference from our previous study was that two different doses of HSM (160 mg/kg/day and 480 mg/kg/day) were used in this experiment. Therefore, the intragastric administration of HSM on the 5th day following the intratracheal instillation with BLM demonstrated reduced collagen deposition and lung fibrosis (Fig. 1B and 1C). In addition, we found that the lung function of the BLM group was abnormal compared with that of the control group, and these symptoms were considerably decreased following HSM treatment (Fig. S1A–S1E). Therefore, HSM relieved the

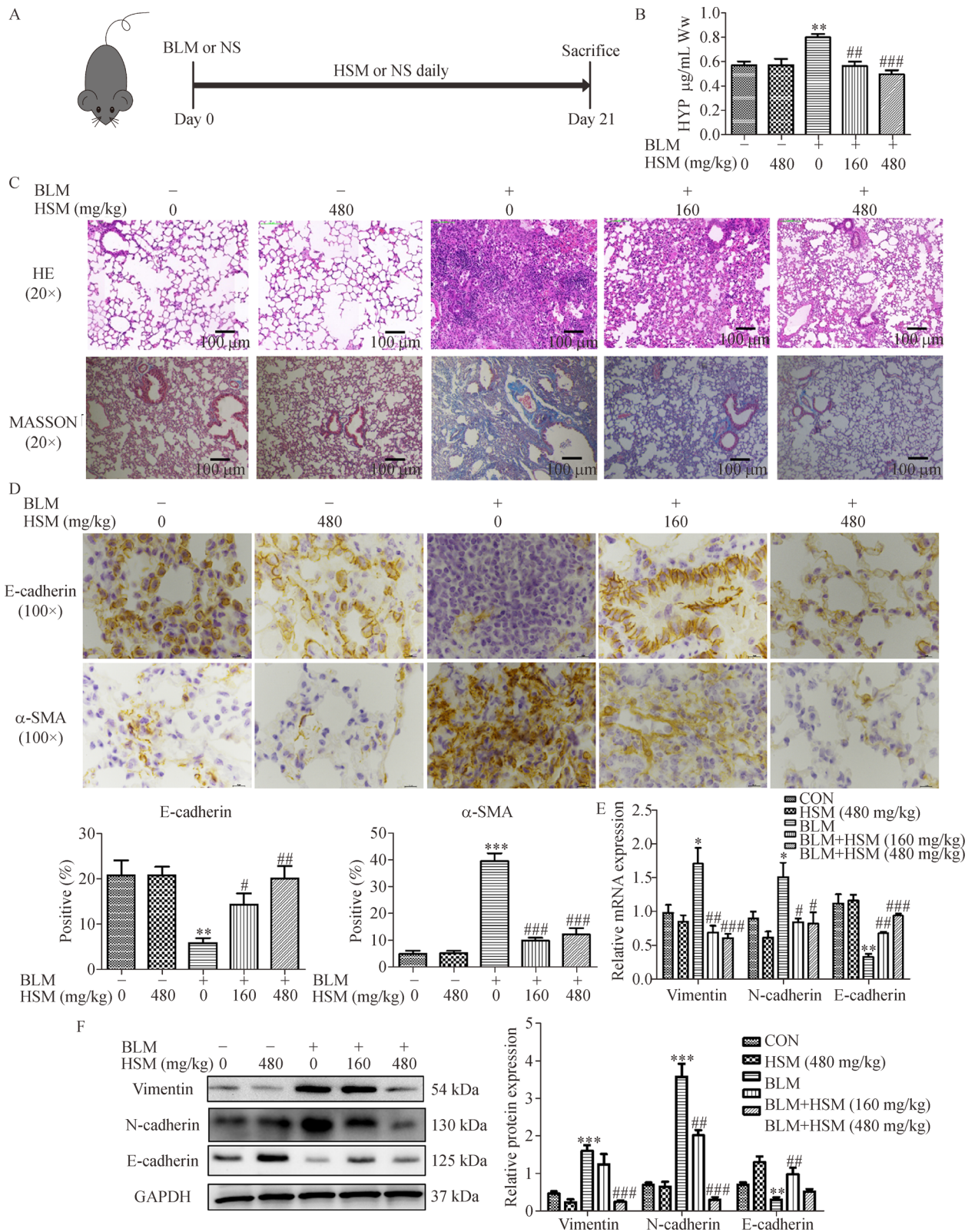


**Fig. 1** HSM alleviated EMT in BLM-treated mice with lung fibrosis. (A) The experimental plan was visualized. (B) Hydroxyproline analysis was performed to quantify the deposition of collagen. (C) H&E staining and Masson staining were used to determine the degree of fibrosis. The scale bar indicated 100 μm in the images (20×). (D) Immunohistochemical staining for the E-cadherin and α-SMA was performed. The scale bar indicated 10 μm in the images (100×). (E) The mRNA levels of vimentin, N-cadherin, and E-cadherin in lung tissues were analyzed through qRT-PCR analyses. (F) The protein levels of vimentin, N-cadherin, and E-cadherin in the lung tissues were analyzed through Western blot analyses. Data represent the mean ± SD of three separate experiments. *n* = 6. \**P* < 0.05, \*\**P* < 0.01, \*\*\**P* < 0.005, vs. control group. #*P* < 0.05, ###*P* < 0.01, ####*P* < 0.005, vs. BLM group.

lung fibrosis induced by BLM.

Previous studies have demonstrated that EMT is one of the important sources of fibroblastic lesion formation in lung tissues [20,21]. To investigate whether HSM played a role in improving lung fibrosis by inhibiting EMT, the cells in the paraffin sections of the lung tissues were labeled with  $\alpha$ -SMA (fibroblast marker) and E-cadherin (epithelial cell marker) by immunohistochemical staining. E-cadherin is a calcium-dependent transmembrane glycoprotein expressed in epithelial cells. Normally, E-cadherin acts as a cell–cell junction to promote intercellular adhesion and maintain cell polarity and histological structure [39,40].  $\alpha$ -SMA is not expressed in normal alveolar epithelial cells, which is mainly expressed as a cytoskeleton in fibroblasts [41,42]. Results indicate that  $\alpha$ -SMA levels were apparently increased in the BLM group, whereas E-cadherin levels were eminently reduced (Fig. 1D). To further confirm the antifibrotic effects of HSM, the expression levels of vimentin, N-cadherin, and E-cadherin were assessed by qRT-PCR and Western blot analyses in mouse lung tissues. Results indicated that the mRNA

and protein expression levels of E-cadherin were apparently decreased. Moreover, the levels of vimentin and N-cadherin were significantly increased (Fig. 1E and 1F). Notably, all the changes were reversed in the HSM treatment group, which indicates that HSM relieved EMT in the lung tissues of mice with pulmonary fibrosis (BLM-induced).

### HSM inhibited the expression levels of midkine in the lung tissues of BLM-induced mice

Midkine demonstrated a critical regulatory role in EMT [34–36]. Therefore, we hypothesized that the anti-EMT effect of HSM was associated with midkine expression levels. The expression levels of midkine in the lung tissues were evaluated through western blotting and qRT-PCR analyses. Findings reveal that the expression levels of this factor remarkably increased in the BLM-induced group. HSM decreased the expression levels of midkine in a dose-dependent manner (Fig. 2A and 2B). Therefore, we assumed that midkine is a potential target of

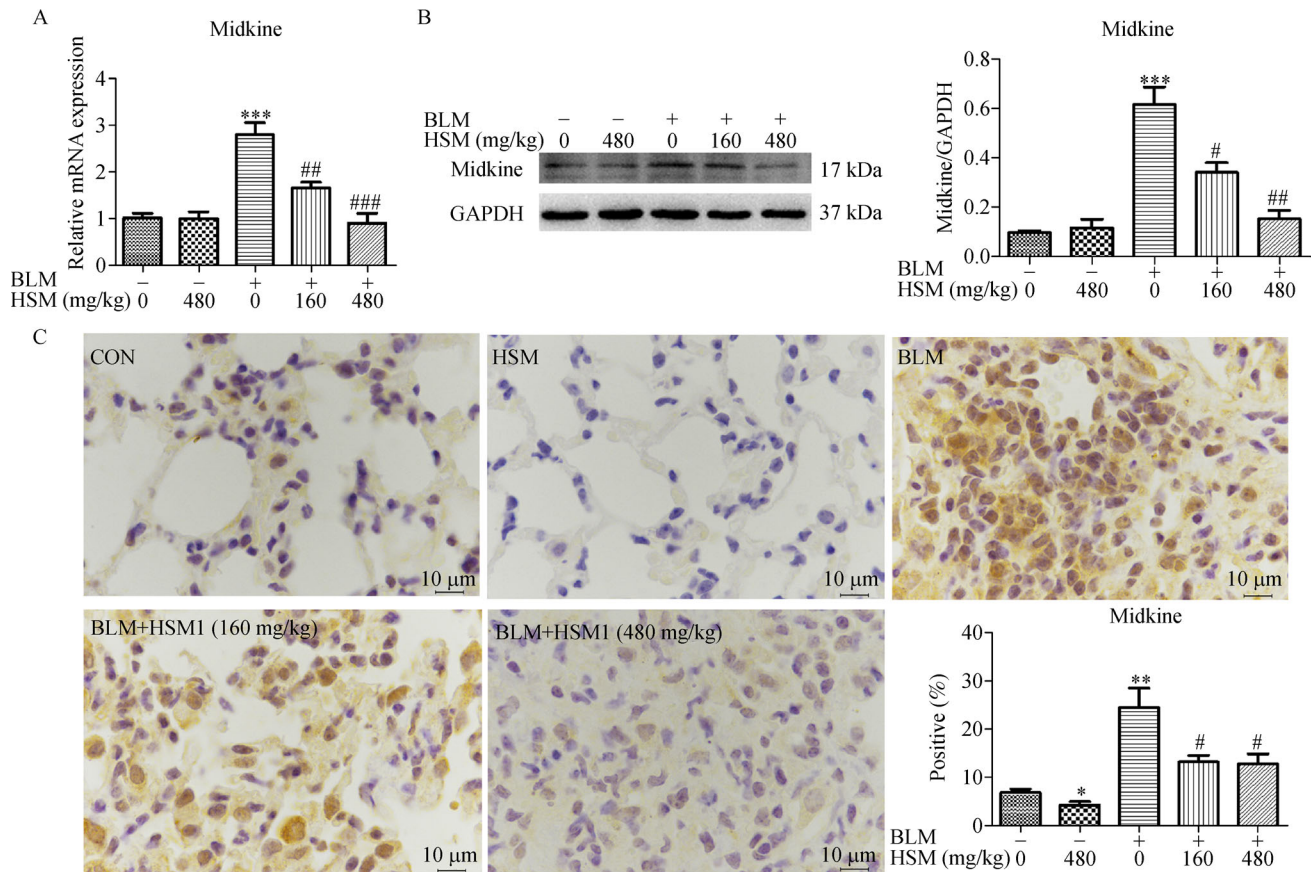


**Fig. 2** HSM inhibited the expression levels of midkine in the lung tissues of BLM-induced mice. (A) The mRNA levels of midkine was performed using qRT-PCR analyses. (B) The protein level of midkine was determined using Western blot analyses. (C) The immunohistochemical staining was performed to determine the expression and location of midkine. The scale bar indicated 10  $\mu$ m in the images (10 $\times$ ). Data represent the mean  $\pm$  SD of three separate experiments.  $n = 6$ . \* $P < 0.05$ , \*\* $P < 0.01$ , \*\*\* $P < 0.005$ , vs. control group. # $P < 0.05$ , ### $P < 0.01$ , #### $P < 0.005$ , vs. BLM group.

HSM-mediated anti-EMT function. Midkine was reported to exhibit low expression in normal adult mouse lung epithelial cells but abnormally increase when lung tissue damage or EMT activation occurs [35]. Signal sequence-less midkine mainly accumulated in the nucleus, whereas signal sequence-containing midkine was detected in the cytoplasm, which was eventually secreted [43]. In our results, immunohistochemical analysis results indicate that midkine was mainly expressed in the nucleus of lung epithelial cells and was secreted into cell gap after BLM treatment. Following the administration of HSM, the secreted midkine was significantly reduced and was mainly concentrated in the nucleus (Fig. 2C).

### The expression levels of midkine were positively associated with EMT activation

To confirm whether the expression levels of midkine were associated with EMT, we further analyzed the correlation between midkine and EMT in the lung tissue. Results indicate that the mRNA expression levels of midkine were positively associated with those of vimentin ( $P < 0.05$ ), N-cadherin ( $P < 0.05$ ), and  $\alpha$ -SMA ( $P < 0.05$ ), while they were negatively associated with E-cadherin levels ( $P < 0.05$ ). Therefore, midkine is positively associated with EMT (Fig. 3A). In addition, we performed experiments *in vitro* to verify this hypothesis. We transfected A549 cells with pcDNA3.1/midkine to overexpress midkine (Fig. S2). A549 cells and mouse primary type II AECs display EMT characteristics after the transfection of the midkine plasmid, such as the increase in mRNA expression levels of vimentin and N-cadherin, and the decrease in E-cadherin expression levels (Fig. 3B). These changes were also confirmed by the Western blot analysis and by immunofluorescence staining (Fig. 3C and 3D, Fig. S5A and S5B). In summary, the positive correlation between midkine and EMT is confirmed *in vitro* and *in vivo*.

### HSM inhibited TGF- $\beta$ 1-induced EMT in A549 cells and mouse primary type II AECs

The CCK8 assay was conducted to detect the maximum toxicity of HSM in the cells. Two doses of HSM (16 and 160  $\mu$ g/mL) were applied for subsequent experiments (Fig. 4A, Fig. S3A). To verify the efficacy of HSM for inhibiting EMT, A549 cells and mouse primary type II AECs were treated with TGF- $\beta$ 1 (5  $\mu$ g/mL) to induce EMT *in vitro*. The cells were subsequently treated with HSM. Results indicate that EMT was induced in A549 cells and in mouse primary type II AECs following TGF- $\beta$ 1 treatment as the mRNA and protein expression levels of E-cadherin were decreased, whereas the mRNA and protein expression levels of vimentin and N-cadherin were increased (Fig. 4B and 4C, Fig. S3B). However, the

treatment with different concentrations of HSM (16 and 160  $\mu$ g/mL) suppressed the induction of EMT by the TGF- $\beta$ 1. In addition, the protein expression levels of collagen and  $\alpha$ -SMA, which are considered mesenchymal markers, indicated an increase in the TGF- $\beta$ 1-induced group, whereas HSM treatment reduced this effect (Fig. 4D, Fig. S3B). Immunofluorescence staining demonstrated that the fluorescence signals of vimentin and  $\alpha$ -SMA were maximal in the TGF- $\beta$ 1-induced group, and they were significantly weakened after an HSM treatment (Fig. 4E, Fig. S3C and Fig. S4). These results indicated that HSM inhibited the TGF- $\beta$ 1-induced EMT *in vitro*.

### HSM inhibited the expression of midkine and its downstream signaling proteins in the TGF- $\beta$ 1-induced EMT model

Based on the aforementioned results, the association between midkine and the antifibrotic effects of HSM on A549 cells and mouse primary type II AECs induced by TGF- $\beta$ 1 was further evaluated. The expression levels of midkine in the TGF- $\beta$ 1 group increased compared with those of the control group, which was consistent with the results noted *in vivo*. After the treatment with HSM, the expression levels of midkine were reduced (Fig. 5A and 5B, Fig. S3B). The expression levels of the protein associated with the signaling pathway of midkine were examined. The data indicated the expression levels of Notch2 and ACE increased in the TGF- $\beta$ 1 group, whereas the expression levels of NOX1 remained unaltered compared with those of the control group (Fig. 5C and 5D, Fig. S3B). The treatment with HSM markedly inhibited these TGF- $\beta$ 1-activated signaling molecules (Fig. 5D). In summary, HSM blocked midkine action and the expression of its associated signaling pathway proteins in the TGF- $\beta$ 1-induced EMT cell model.

### HSM inhibited induction of EMT by midkine overexpression in A549 cells and in mouse primary type II AECs

To determine whether HSM inhibited EMT by decreasing the expression of midkine, we constructed a midkine-overexpressing A549 cell line and a midkine-overexpression mouse primary type II AECs by transfecting these cells with pcDNA3.1/midkine. The successful transfection indicates that pcDNA3.1/midkine induced an upregulated midkine expression in A549 cells and in mouse primary type II AECs compared with vehicle group, and HSM reversed these upregulation (Fig. 6A–6C, Fig. S5A). Furthermore, results indicate that the expression levels of the signaling pathway proteins associated with midkine (NOX1, Notch2, and ACE) in the pcDNA3.1/midkine transfection group increased, whereas the expression levels

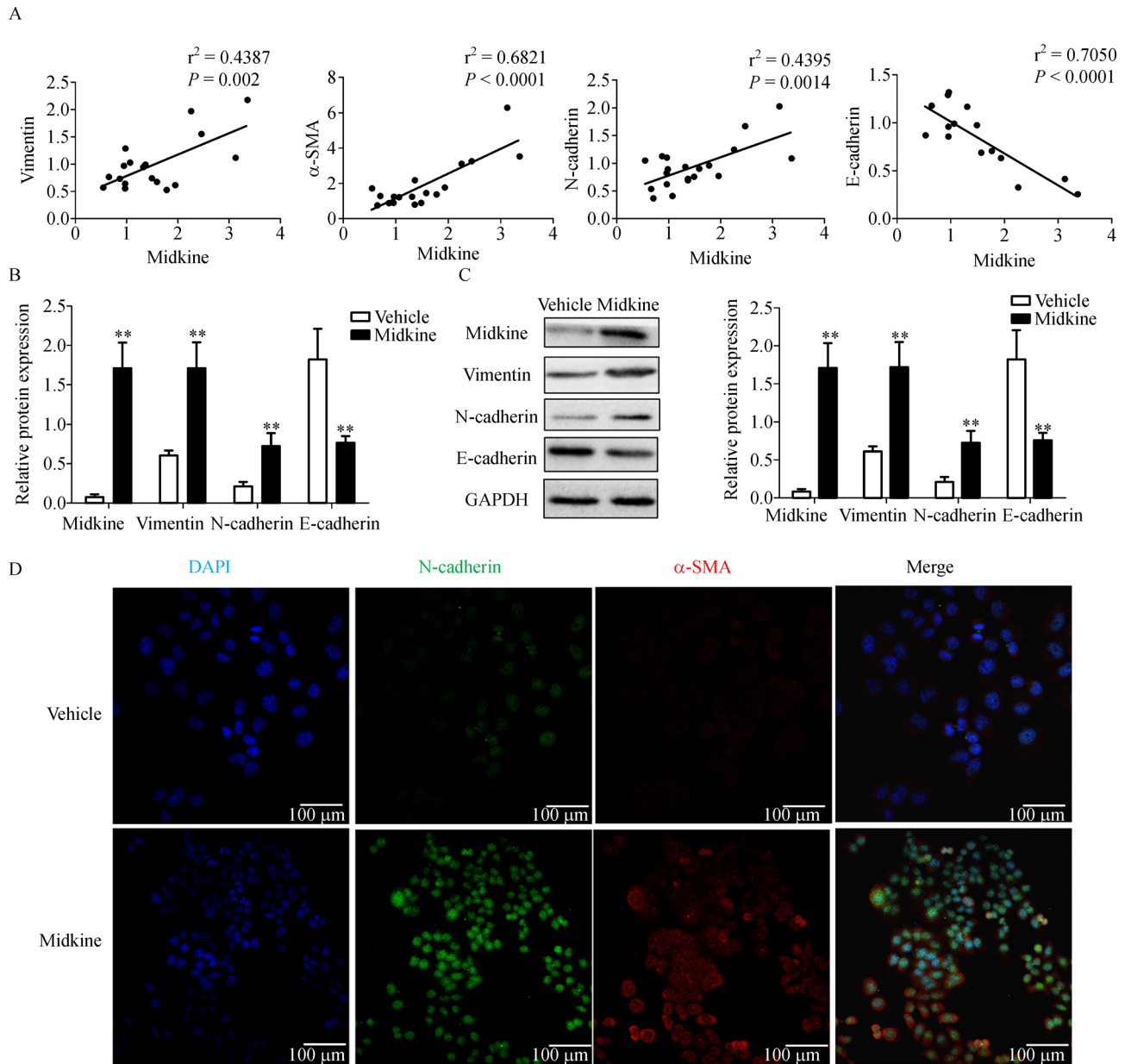


**Fig. 3** The expression levels of midkine were positively associated with EMT activation. (A) The correlation between midkine and EMT markers ( $\alpha$ -SMA, vimentin, N-cadherin, and E-cadherin) in the lung tissue. (B) A549 cells were transfected with pcDNA3.1/midkine plasmid, and mRNA expression levels of midkine, vimentin, N-cadherin, and E-cadherin were determined using qRT-PCR analyses. (C) The protein levels of midkine, vimentin, N-cadherin, and E-cadherin were analyzed by Western blot analyses. (D) The expression of N-cadherin and  $\alpha$ -SMA were analyzed by immunofluorescence staining. The scale bar indicated 100  $\mu$ m in the images (40 $\times$ ). Data represent the mean  $\pm$  SD of three separate experiments.  $n = 6$ . \*\* $P < 0.01$ , vs. vehicle group.

of Notch2 and ACE significantly decreased after the HSM treatment (Fig. 6D and 6E, Fig. S5A, Fig. S6). Notably, no difference is evident in NOX1 levels between the transfected and the vehicle groups (Fig. 6D and 6E, Fig. S5A).

The expression levels of classical EMT markers were investigated. Results indicated that vimentin, N-cadherin, collagen, and  $\alpha$ -SMA levels increased, whereas the levels

of E-cadherin decreased, which confirmed that midkine resulted in EMT activation. Subsequently, the cells were treated with HSM (160  $\mu$ g/mL). Results demonstrated that the intervention of HSM relieved EMT in midkine-overexpressing cells, whereas the changes noted in the epithelial and mesenchymal markers were reversed (Fig. 7A–7C, Fig. S5A). Immunofluorescence staining further proved that HSM could relieve EMT by inhibiting

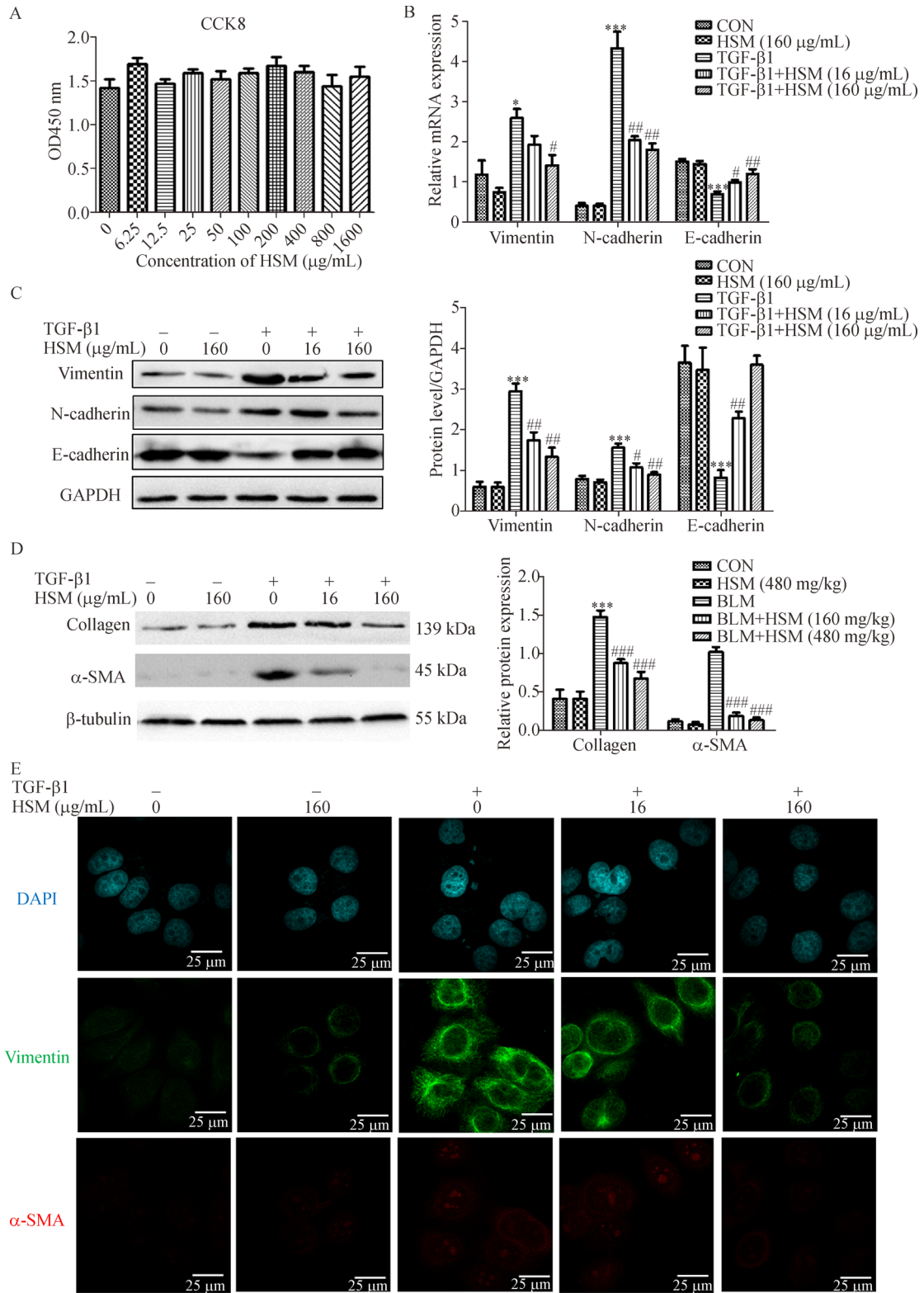


**Fig. 4** HSM inhibited TGF- $\beta$ 1-induced EMT in A549 cells. (A) A549 cells were treated with various concentrations of HSM and cultured for 24 hours. The cell viability was analyzed by the CCK8 assay. A549 cells were pretreated with HSM for 2 hours and were subsequently treated with or without TGF- $\beta$ 1 (5 ng/mL) for 24 hours. (B) The mRNA levels of vimentin, E-cadherin, and N-cadherin were analyzed through qRT-PCR analyses. (C) The protein levels of vimentin, E-cadherin, and N-cadherin were performed using Western blot analyses. (D) The protein levels of  $\alpha$ -SMA and collagen were performed using Western blot analyses. (E) The expression of EMT markers (vimentin and  $\alpha$ -SMA) were analyzed by immunofluorescence staining. The scale bar indicated 25  $\mu\text{m}$  in the images (100 $\times$ ). Data represent the mean  $\pm$  SD of three separate experiments \* $P < 0.05$ , \*\*\* $P < 0.005$ , vs. control group. # $P < 0.05$ , ### $P < 0.01$ , #### $P < 0.005$ , vs. BLM group.

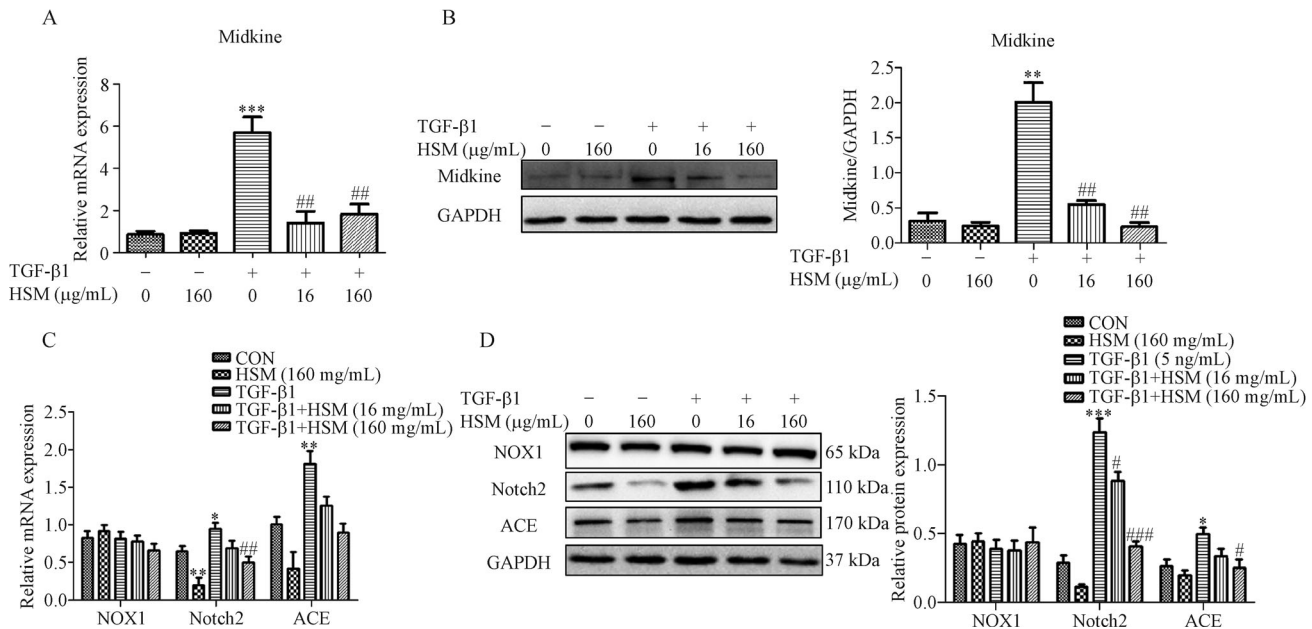


**Fig. 5** HSM inhibited the expression of midkine and its downstream signaling proteins in the TGF-β1-induced EMT model. A549 cells were pretreated with HSM for 2 hours and treated with or without TGF-β (5 ng/mL) for 24 hours. The mRNA levels of midkine (A), NOX1, Notch2, and ACE (C) were analyzed through qRT-PCR analyses. The protein levels of midkine (B), NOX1, Notch2, and ACE (D) were analyzed by Western blot analyses. Data represent the mean  $\pm$  SD of three separate experiments. \* $P < 0.05$ , \*\* $P < 0.01$ , \*\*\* $P < 0.005$ , vs. control group. # $P < 0.05$ , ## $P < 0.01$ , ### $P < 0.005$ , vs. BLM group.

the expression of midkine (Fig. 7D, Fig. S5B).

### HSM inhibited BLM-induced midkine signaling pathway activation *in vivo*

We demonstrated that HSM reduced the expression levels of Notch2 and ACE by downregulating midkine levels *in vitro*. Similar results were found in the mouse model demonstrating that the expression levels of NOX1, Notch2, and ACE in BLM-treated mice were increased (Fig. 8A and 8B). These changes were reversed after the HSM treatment. Therefore, HSM exhibited antifibrotic effects by interacting with midkine to inhibit EMT.

In summary, the treatment of alveolar epithelial cells with HSM downregulated the expression levels of Notch2 and ACE via midkine, while it further reduced the induction of EMT and alleviated IPF.

## Discussion

The present study demonstrates that the midkine pathway may be a novel candidate for therapeutic target of HSM for BLM-induced lung fibrosis by regulating the EMT. This assumption was confirmed by the effect of HSM on lung fibrosis and on the induction of EMT in BLM-treated mice and in TGF-1β-treated A549 cells and mouse primary type II AECs *in vitro*. Midkine overexpression induced EMT in

A549 cells and mouse primary type II AECs while activating its downstream signaling pathway of the induction of EMT. Moreover, the levels of midkine were reduced by HSM treatment concomitantly, which suggests that HSM may alleviate pulmonary fibrosis by targeting midkine.

BLM-induced pulmonary fibrosis is characterized by inflammation and fibrosis in lung tissues. Based on the murine BLM-induced pulmonary fibrosis model, we evaluated the antifibrotic effects of the potential therapeutic agent *H. sinensis* that is used as an alternative to *Cordyceps sinensis*. HSM has demonstrated a variety of biological activities, including antitumor, immunoregulatory, anti-inflammatory, antioxidative, anti-infective, and anti-aging activities [13]. Previous studies have recently demonstrated the antifibrotic activity of HSM, whereas the underlying molecular mechanism remained unknown [11,12,15,16].

The present results reveal that HSM alleviated lung fibrosis and EMT *in vitro* and *in vivo*. EMT is considered as a process of extreme epithelial cell plasticity. The production of fibroblasts is essential for the formation of pulmonary fibrosis because these cells are mainly responsible for the augmented collagen and increased matrix synthesis and deposition that occur in the process of pulmonary fibrosis [44]. In the present study, we detected a significant increase in the levels of fibroblast markers (vimentin and N-cadherin) in the lung tissue of BLM-

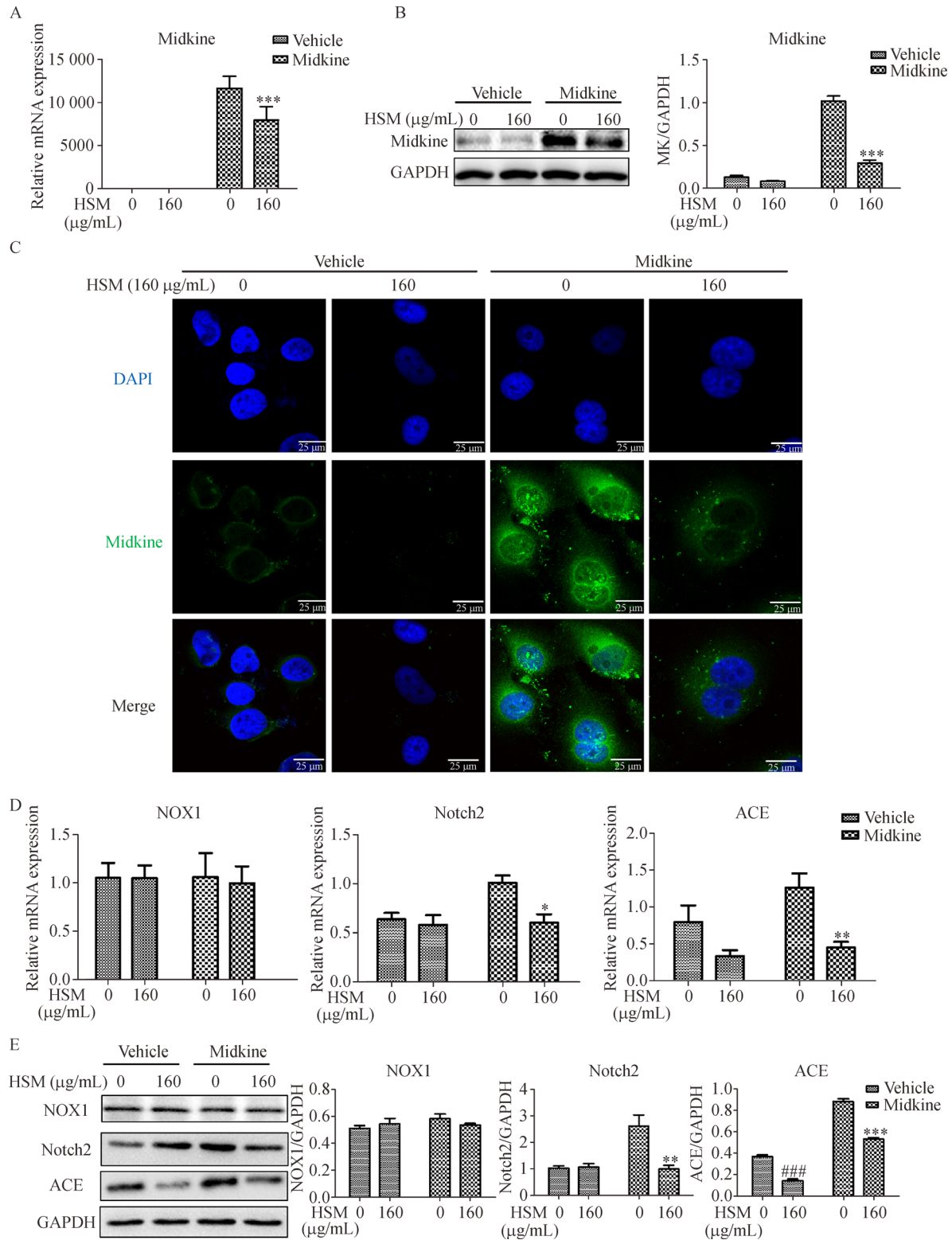


**Fig. 6** HSM inhibited induction of EMT by midkine overexpression in A549 cells. A549 cells were pretreated with HSM for 2 hours and then transfected with pcDNA3.1/midkine plasmid. (A) The mRNA expression of midkine was analyzed through qRT-PCR analyses. (B) The protein levels of midkine was analyzed using Western blot analyses. (C) The expression of midkine was analyzed by immunofluorescence staining. The scale bar indicated 25 μm in the images (100×). (D) The mRNA expression of NOX1, Notch2, and ACE were analyzed using qRT-PCR analyses. (E) The protein levels of NOX1, Notch2, and ACE were performed by Western blot analyses. Data represent the mean ± SD of three separate experiments. ###*P* < 0.005, vs. vehicle group without HSM treatment. \**P* < 0.05, \*\**P* < 0.01, \*\*\**P* < 0.005, vs. transfected with pcDNA/midkine but without HSM treatment group.

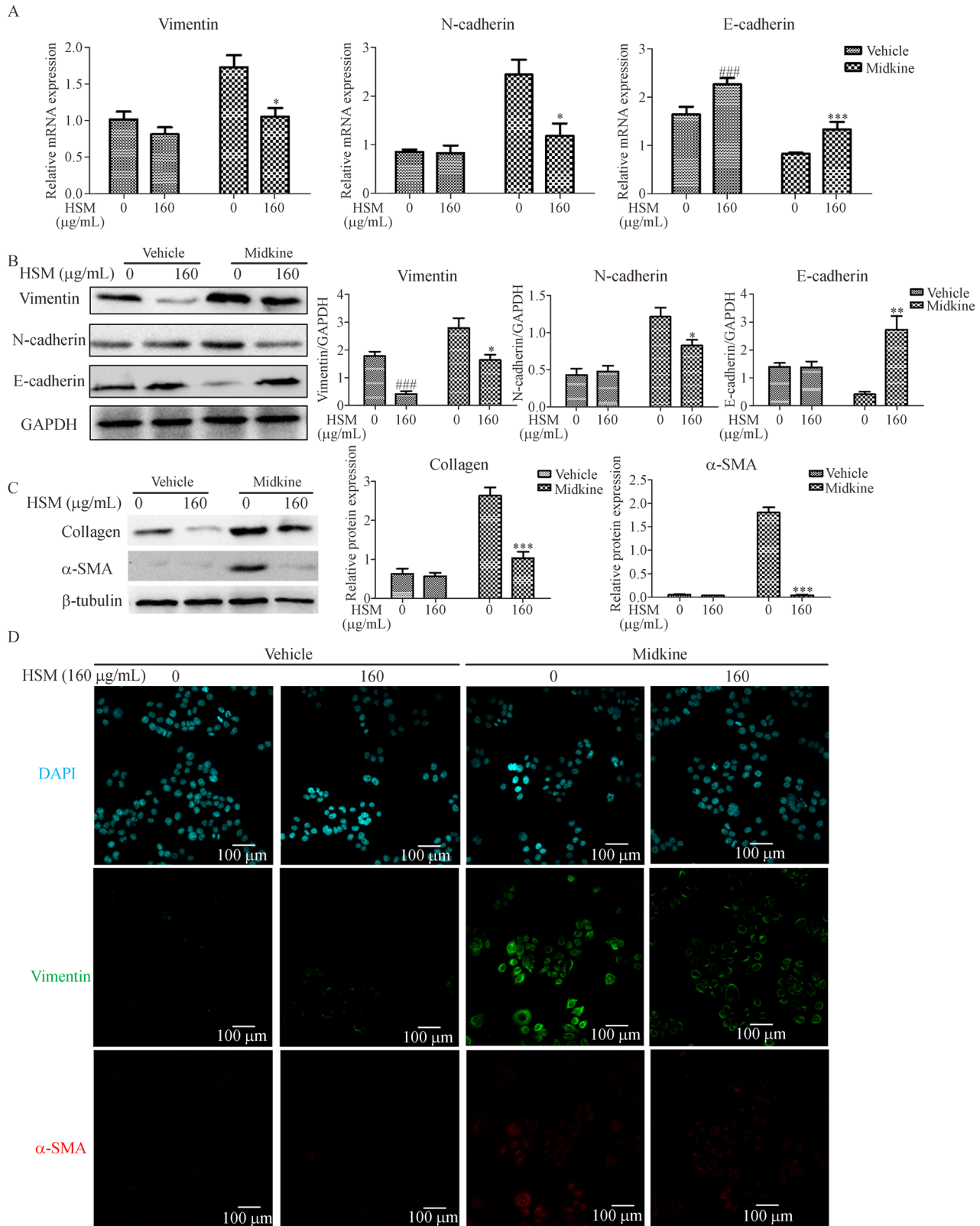


**Fig. 7** HSM inhibited BLM-induced midkine signaling pathway activation *in vivo*. A549 cells were pretreated with HSM for 2 hours and were subsequently transfected with pcDNA3.1/midkine plasmid. (A) The mRNA expression of vimentin, N-cadherin, and E-cadherin were analyzed using qRT-PCR analyses. (B) The protein levels of vimentin, N-cadherin, and E-cadherin were performed using Western blot analyses. (C) The expression of vimentin and  $\alpha$ -SMA were analyzed by immunofluorescence staining. The scale bar indicated 100  $\mu$ m in the images (40 $\times$ ). Data represent the mean  $\pm$  SD of three separate experiments. ### $P$  < 0.005, vs. vehicle group without HSM treatment. \* $P$  < 0.05, \*\* $P$  < 0.01, \*\*\* $P$  < 0.005, vs. transfected with pcDNA/midkine but without HSM treatment group.

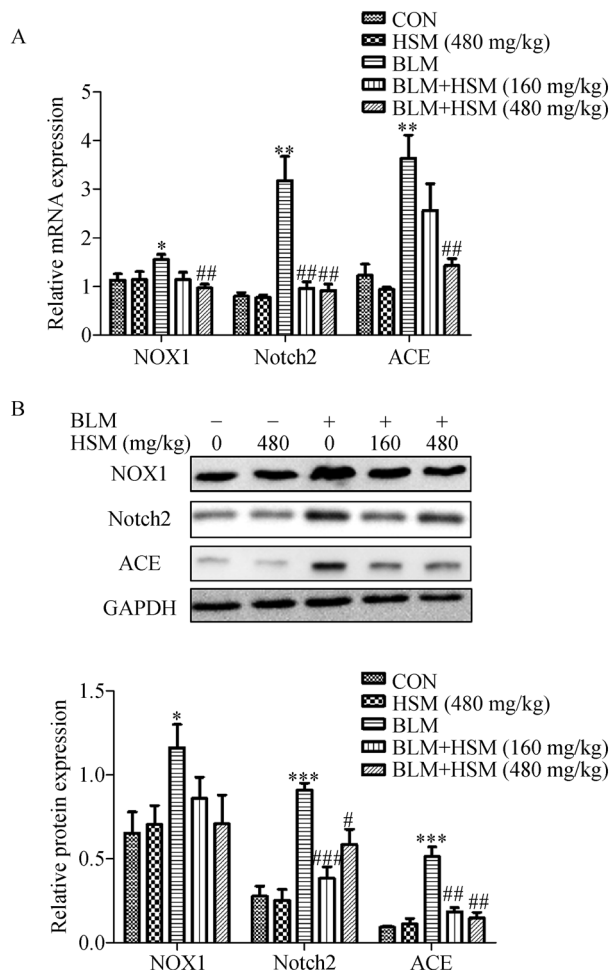


**Fig. 8** HSM inhibited BLM-induced midkine signaling pathway activation *in vivo*. (A) The mRNA levels of NOX1, Notch2, and ACE in mouse lung tissue were analyzed using real-time PCR. (B) The protein levels of NOX1, Notch2, and ACE in the mouse lung tissue were analyzed by Western blot analyses. Data represent the mean  $\pm$  SD of three separate experiments. \* $P < 0.05$ , \*\* $P < 0.01$ , \*\*\* $P < 0.005$ , vs. control group. # $P < 0.05$ , ## $P < 0.01$ , ### $P < 0.005$ , vs. BLM group.

induced mice. Thus, the fibroblasts were proliferating abnormally. H&E and Masson staining further confirmed the damage of lung tissues and the collagen deposition among BLM-induced mice, which was consistent with the majority of relevant studies [45–47]. However, the origin of lung fibroblasts during pulmonary fibrosis has not been defined well. Owing to the various sources of fibroblasts, different hypotheses explaining the etiology of this disease have been proposed including the proliferation of resident lung interstitial fibroblasts, differentiation of progenitor cells from the bone marrow, and transition of epithelial cells to a fibroblast phenotype, which is a process termed EMT [48]. The notion that EMT contributes to organ fibrosis has received considerable attention. Particular focus has been paid to determining the extent of the contribution of EMT to the fibroblastic and myofibroblas-

tic lung population [49]. Since 2009, Tanjore *et al.* demonstrated that after the BLM treatment for two weeks, approximately one-third of the lung fibroblasts in mouse lung tissue were epithelial pedigrees, whereas the resident interstitial cells were the key contributors to the lung fibroblast population [50]. In the same year (2009), Kim *et al.* further demonstrated that on day 17 following BLM administration, 8.9% of GFP<sup>+</sup> cells (indicating all epithelial-derived cells) expressed vimentin, 5.3% expressed  $\alpha$ -SMA and 4.8% collagen-1 [51]. Although EMT was not a major source of lung fibroblasts, it also played an important role in the formation of pulmonary fibrosis [17,18]. In the present study, we demonstrated that EMT was induced in mouse lung after the BLM treatment. HSM treatment attenuated the transition of alveolar epithelial cells into fibroblasts. The accumulation of fibroblasts was a typical feature of pulmonary fibrosis, and its reduction indicated that pulmonary fibrosis was alleviated. Thus, HSM prevented the transition of epithelial cells into fibroblasts and subsequently reduced the development of pulmonary fibrosis. We also used TGF- $\beta$ 1 to induce the EMT model in A549 cells and primary type II AECs. A safe dose of HSM (16  $\mu$ g/mL and 160  $\mu$ g/mL) was applied. Results indicate that EMT was induced in TGF- $\beta$ 1-treated cells, along with the increased expression of vimentin and N-cadherin, and with the decreased expression of E-cadherin. These changes were alleviated following treatment with different concentrations of HSM. In summary, HSM could inhibit EMT *in vivo* and *in vitro*.

We further observed that midkine inactivation and EMT induction were reduced by HSM treatment. Although midkine is recently considered a hotspot in cancer research, merely a limited number of studies have been conducted with regard to fibrosis or EMT. In 2008, Huang *et al.* first proposed that midkine could induce EMT via Notch2/Jak2-Stat3 signaling pathway. Although glial cells were used in that study instead of epithelial cells, data demonstrated the association between EMT and the expression of midkine in keratinocyte cell lines [52]. In 2017, a study highlighted that midkine was involved in the development of pulmonary fibrosis and demonstrated that its serum levels among patients with IPF and mouse BAL fluid were significantly increased [53]. Although the exact mechanism regarding midkine levels and the induction of EMT is not completely discovered, this factor has been involved in the development of pulmonary fibrosis. A recent study on ARDS demonstrated the association between midkine and fibrosis. The authors concluded that midkine was highly expressed in the lungs of ARDS patients and that the induction of fibrosis was reduced among midkine<sup>-/-</sup> mice. Furthermore, the signaling proteins activated in response to midkine were identified as NOX1, midkine, Notch2, and ACE [32,33]. Although ARDS-induced fibrosis may differ from BLM-induced

fibrosis, these observations were meaningful for the investigation of pulmonary fibrosis and the involvement of midkine in that process. We demonstrated that the mRNA and protein levels of midkine were upregulated in the lung tissue of BLM group compared with control group, whereas HSM treatment effectively inhibited the expression of midkine. In addition, the proteins of the midkine signaling pathway exhibited a similar tendency with regard to their expression levels. Moreover, the expression levels of midkine and the signaling pathway associated protein were investigated in TGF- $\beta$ 1 treated A549 cells and in mouse primary type II AECs. qRT-PCR and Western blot analyses revealed that the expression levels of midkine, Notch2, and ACE were increased in the TGF- $\beta$ 1-induced group compared with those noted in the control group, whereas HSM treatment reduced these expression levels. We further verified whether the expression of midkine exhibited a synergistic association with the incidence of EMT in the epithelial cells, and whether HSM could inhibit the development of EMT by targeting midkine.

In the present study, we performed a correlation analysis between the gene expression of midkine and the expression of specific EMT markers. Correlation analysis indicated that the incidence of EMT correlated positively with the activation of midkine. In addition, midkine correlated positively with the expression levels of vimentin, N-cadherin, and  $\alpha$ -SMA but correlated negatively with the expression levels of E-cadherin. In 2011, G $\ddot{u}$ ng $\ddot{o}$ r *et al.* proposed the idea that midkine induced EMT in pancreatic cancer by activating the Notch protein [34]. This study demonstrated that midkine depletion induced the reversal of EMT in L3.6pl-Res cells [34]. Subsequent studies by Zhao *et al.* demonstrated that estradiol enhanced the EMT of lung adenocarcinoma cells by increasing the transcription of midkine. This study describes the mechanism of how estradiol regulated the expression levels of midkine and further mediated the development of EMT [35]. The two aforementioned studies demonstrated that midkine exerted a pro-EMT role. To further investigate whether midkine was a potential target of HSM, we transfected A549 cells and mouse primary type II AECs with a pcDNA3.1/midkine plasmid to increase the expression levels of this protein and in turn activate EMT. Subsequently, we examined the expression of EMT markers and proved that EMT was induced after a successful transfection of the pcDNA3.1/midkine plasmid in A549 cells and in mouse primary type II AECs. This finding indicates that upregulation of midkine activated EMT, while the expression levels of specific epithelial markers were increased after the treatment with HSM. In contrast to the epithelial markers, the expression levels of specific mesenchymal markers were decreased. Moreover, the mRNA and protein levels of Notch2 and ACE were increased following overexpression of midkine. However,

these changes were reversed by the treatment with HSM. Results suggested that HSM may block the development of EMT by targeting midkine.

The expression levels of NOX1 remained unaltered in TGF- $\beta$ 1-induced EMT and in midkine overexpressed cells. The involvement of NOX1 in the development of fibrosis or in the induction of EMT has not been fully characterized. Zhang *et al.* revealed that mechanical stretching activates the NOX1-midkine-Notch2-ACE signaling pathway, which further induced the occurrence of the EMT. The authors suggested that NOX1 may be the upstream protein of midkine [33]. Liu *et al.* demonstrated that NOX1 overexpression enhanced invasion via the matrix metalloproteinase-2 (MMP2) and activated the EMT in melanoma cells, thereby indicating that overexpression of NOX1 could regulate the development of EMT in melanocytes [54]. Furthermore, Kesanakurti *et al.* proposed that PAK4 and PPAR $\gamma$  could be gathered together to the NOX1 promoter, thereby yielding an upregulation of NOX1 transcription. The effect resulted in additional ROS production and consequently induced EMT in cells [55]. The aforementioned studies indicated that NOX1 may participate in the development of EMT via other pathways. In the present study, the data indicated upregulation of NOX1 in BLM treated lung tissue. HSM suppressed these effects *in vitro*. In 2016, Das *et al.* highlighted that TGF- $\beta$ 1 treatment could induce the expression and activity of NOX4 (but not NOX1-3) in rat lens epithelial explants and further induce the incidence of EMT [56]. After 8 hours of TGF- $\beta$ 1 treatment, NOX4 could be observed in the nucleus, and it was mainly colocalized with  $\alpha$ -SMA during the late stage of EMT (48 h) [56]. Inhibition of NOX4 expression alleviated EMT induction [56]. These findings may explain the lack of changes in the NOX1 expression *in vitro*.

The present study presents that HSM blocked the development of EMT by targeting midkine and thus alleviated lung fibrosis in BLM-treated mice. Nevertheless, the present study exhibits several limitations. Initially, we focused on the antifibrotic effects of HSM, which mitigated EMT and further attenuated IPF injury by inhibiting the midkine signaling pathway. However, we failed to examine the antifibrotic effects in midkine knockout mice. Finally, HSM is a complex Chinese herbal extract, and several of its components may be involved in complicated regulatory mechanisms, which required further investigation [57,58].

The current findings can be substantiated by future studies, which may determine the exact interactions of NOX1 with the induction of EMT. In particular, we demonstrated that NOX1 was upregulated in the BLM-induced animal model compared with the corresponding levels in the control groups and that NOX1 was downregulated after HSM administration. However, the levels of NOX1 were not elevated in TGF- $\beta$ 1-induced and plasmid-

transfected A549 cells and in mouse primary type II AECs, while HSM cannot decrease the expression of NOX1. Previous studies have shown that a complex regulatory mechanism was involved in NOX1. The induction of NOX1 was required for normal development, which may occur in the mitochondria via a ROS-dependent pathway [59]. Furthermore, an interaction between NOX1 and Bcl-2 has been demonstrated in lung epithelial cells [60]. In summary, the present data implied that in addition to midkine, HSM regulated the expression levels of other NOX1-related genes or proteins. However, this hypothesis requires further investigation.

## Conclusions

The present study demonstrates that HSM treatment effectively improved the BLM-induced lung fibrosis in mice and alleviated the occurrence of EMT in lung tissue. Therefore, the present study suggests that midkine may be an important therapeutic mediator required for the antifibrotic effects of HSM.

## Acknowledgements

The present work is supported by the Six Talent Peaks Project in Jiangsu Province (No. YY-021), the Fundamental Research Funds of the Central Universities (No. 021414380342), and the Fund of State Key Laboratory of Trauma Burns and Combined Injury (No. SKLKF201602). We are also very grateful to Dr. Lizhi Xu (Medical school, Nanjing University) for her technical support.

## Compliance with ethics guidelines

Li Lu, Haiyan Zhu, Hailin Wang, Huaping Liang, Yayi Hou, and Huan Dou declare that they have no conflict of interest. All institutional and national guidelines for the care and use of laboratory animals were followed.

**Electronic Supplementary Material** Supplementary material is available in the online version of this article at <https://doi.org/10.1007/s11684-020-0737-1> and is accessible for authorized users.

## References

- Richeldi L, Collard HR, Jones MG. Idiopathic pulmonary fibrosis. *Lancet* 2017; 389(10082): 1941–1952
- Barratt SL, Creamer A, Hayton C, Chaudhuri N. Idiopathic pulmonary fibrosis (IPF): an overview. *J Clin Med* 2018; 7(8): E201
- Funke M, Geiser T. Idiopathic pulmonary fibrosis: the turning point is now! *Swiss Med Wkly* 2015; 145: w14139
- Kim ES, Keating GM. Pirfenidone: a review of its use in idiopathic pulmonary fibrosis. *Drugs* 2015; 75(2): 219–230
- Richeldi L, du Bois RM, Raghu G, Azuma A, Brown KK, Costabel U, Cottin V, Flaherty KR, Hansell DM, Inoue Y, Kim DS, Kolb M, Nicholson AG, Noble PW, Selman M, Taniguchi H, Brun M, Le Maulf F, Girard M, Stowasser S, Schlenker-Herceg R, Disse B, Collard HR; INPULSIS Trial Investigators. Efficacy and safety of nintedanib in idiopathic pulmonary fibrosis. *N Engl J Med* 2014; 370(22): 2071–2082
- Meyer KC, Decker CA. Role of pirfenidone in the management of pulmonary fibrosis. *Ther Clin Risk Manag* 2017; 13: 427–437
- Richeldi L, Cottin V, Flaherty KR, Kolb M, Inoue Y, Raghu G, Taniguchi H, Hansell DM, Nicholson AG, Le Maulf F, Stowasser S, Collard HR. Design of the INPULSIS™ trials: two phase 3 trials of nintedanib in patients with idiopathic pulmonary fibrosis. *Respir Med* 2014; 108(7): 1023–1030
- Hajari Case A, Johnson P. Clinical use of nintedanib in patients with idiopathic pulmonary fibrosis. *BMJ Open Respir Res* 2017; 4(1): e000192
- Zhu JS, Halpern GM, Jones K. The scientific rediscovery of an ancient Chinese herbal medicine: *Cordyceps sinensis*: part I. *J Altern Complement Med* 1998; 4(3): 289–303
- Zhu JS, Halpern GM, Jones K. The scientific rediscovery of a precious ancient Chinese herbal regimen: *Cordyceps sinensis*: part II. *J Altern Complement Med* 1998; 4(4): 429–457
- Huang TT, Chong KY, Ojcius DM, Wu YH, Ko YF, Wu CY, Martel J, Lu CC, Lai HC, Young JD. *Hirsutella sinensis* mycelium suppresses interleukin-1 $\beta$  and interleukin-18 secretion by inhibiting both canonical and non-canonical inflammasomes. *Sci Rep* 2013; 3(1): 1374
- Huang TT, Lai HC, Ko YF, Ojcius DM, Lan YW, Martel J, Young JD, Chong KY. *Hirsutella sinensis* mycelium attenuates bleomycin-induced pulmonary inflammation and fibrosis *in vivo*. *Sci Rep* 2015; 5(1): 15282
- Koh JH, Yu KW, Suh HJ, Choi YM, Ahn TS. Activation of macrophages and the intestinal immune system by an orally administered decoction from cultured mycelia of *Cordyceps sinensis*. *Biosci Biotechnol Biochem* 2002; 66(2): 407–411
- Nordin SL, Jovic S, Kurut A, Andersson C, Gela A, Bjartell A, Mrgelin M, Olin AI, Lund M, Egesten A. High expression of midkine in the airways of patients with cystic fibrosis. *Am J Respir Cell Mol Biol* 2013; 49(6): 935–942
- Shou QY, Fu HY, Zhang LZ, Cai YQ, Chen FM, Chen ML. Study on treatment effect and mechanism of *Hirsutella sinensis* mycelium in idiopathic pulmonary fibrosis in rats. *China J Chin Mater Med (Zhongguo Zhong Yao Za Zhi)* 2012; 37(23): 3618–3623 (in Chinese)
- Yue H, Zhao Y, Wang H, Ma F, Liu F, Shen S, Hou Y, Dou H. Anti-fibrosis effect for *Hirsutella sinensis* mycelium based on inhibition of mTOR p70S6K phosphorylation. *Innate Immun* 2017; 23(7): 615–624
- Chen B, Cai HR, Xue S, You WJ, Liu B, Jiang HD. Bile acids induce activation of alveolar epithelial cells and lung fibroblasts through farnesoid X receptor-dependent and independent pathways. *Respirology* 2016; 21(6): 1075–1080
- O’Beirne SL, Walsh SM, Fabre A, Reviriego C, Worrell JC, Counihan IP, Lumsden RV, Cramton-Barnes J, Belperio JA, Donnelly SC, Boylan D, Marchal-Somme J, Kane R, Keane MP. CXCL9 regulates TGF- $\beta$ 1-induced epithelial to mesenchymal transition in human alveolar epithelial cells. *J Immunol* 2015; 195

- (6): 2788–2796
19. Wang YC, Liu JS, Tang HK, Nie J, Zhu JX, Wen LL, Guo QL. miR221 targets HMGA2 to inhibit bleomycin-induced pulmonary fibrosis by regulating TGF $\beta$ 1/Smad3-induced EMT. *Int J Mol Med* 2016; 38(4): 1208–1216
  20. Willis BC, Borok Z. TGF- $\beta$ -induced EMT: mechanisms and implications for fibrotic lung disease. *Am J Physiol Lung Cell Mol Physiol* 2007; 293(3): L525–L534
  21. Kage H, Borok Z. EMT and interstitial lung disease: a mysterious relationship. *Curr Opin Pulm Med* 2012; 18(5): 517–523
  22. Xiao X, Huang C, Zhao C, Gou X, Senavirathna LK, Hinsdale M, Lloyd P, Liu L. Regulation of myofibroblast differentiation by miR-424 during epithelial-to-mesenchymal transition. *Arch Biochem Biophys* 2015; 566: 49–57
  23. Zhang H, Okamoto M, Panzhinskiy E, Zawada WM, Das M. PKC $\delta$ /midkine pathway drives hypoxia-induced proliferation and differentiation of human lung epithelial cells. *Am J Physiol Cell Physiol* 2014; 306(7): C648–C658
  24. Weckbach LT, Preissner KT, Deindl E. The role of midkine in arteriogenesis, involving mechanosensing, endothelial cell proliferation, and vasodilation. *Int J Mol Sci* 2018; 19(9): E2559
  25. Masuda T, Maeda K, Sato W, Kosugi T, Sato Y, Kojima H, Kato N, Ishimoto T, Tsuboi N, Uchimura K, Yuzawa Y, Maruyama S, Kadomatsu K. Growth factor midkine promotes T-cell activation through nuclear factor of activated T cells signaling and Th1 cell differentiation in lupus nephritis. *Am J Pathol* 2017; 187(4): 740–751
  26. Mitsiadis TA, Muramatsu T, Muramatsu H, Thesleff I. Midkine (MK), a heparin-binding growth/differentiation factor, is regulated by retinoic acid and epithelial-mesenchymal interactions in the developing mouse tooth, and affects cell proliferation and morphogenesis. *J Cell Biol* 1995; 129(1): 267–281
  27. Erdogan S, Turkekul K, Dibirdik I, Doganlar O, Doganlar ZB, Bilir A, Oktem G. Midkine downregulation increases the efficacy of quercetin on prostate cancer stem cell survival and migration through PI3K/AKT and MAPK/ERK pathway. *Biomed Pharmacother* 2018; 107: 793–805
  28. Vieceli FM, Bronner ME. Leukocyte receptor tyrosine kinase interacts with secreted midkine to promote survival of migrating neural crest cells. *Development* 2018; 145(20): dev164046
  29. Konishi N, Nakamura M, Nakaoka S, Hiasa Y, Cho M, Uemura H, Hirao Y, Muramatsu T, Kadomatsu K. Immunohistochemical analysis of midkine expression in human prostate carcinoma. *Oncology* 1999; 57(3): 253–257
  30. Netsu S, Shishido T, Kitahara T, Honda Y, Funayama A, Narumi T, Kadowaki S, Takahashi H, Miyamoto T, Arimoto T, Nishiyama S, Watanabe T, Woo CH, Takeishi Y, Kubota I. Midkine exacerbates pressure overload-induced cardiac remodeling. *Biochem Biophys Res Commun* 2014; 443(1): 205–210
  31. Nordin SL, Jovic S, Kurut A, Andersson C, Gela A, Bjartell A, Mrgelin M, Olin AI, Lund M, Egesten A. High expression of midkine in the airways of patients with cystic fibrosis. *Am J Respir Cell Mol Biol* 2013; 49(6): 935–942
  32. Siempos II, Choi AM. Midkine: in the middle of the pathogenesis of acute respiratory distress syndrome-associated lung fibrosis? *Am J Respir Crit Care Med* 2015; 192(3): 271–272
  33. Zhang R, Pan Y, Fanelli V, Wu S, Luo AA, Islam D, Han B, Mao P, Ghazarian M, Zeng W, Spieth PM, Wang D, Khang J, Mo H, Liu X, Uhlig S, Liu M, Laffey J, Slutsky AS, Li Y, Zhang H. Mechanical stress and the induction of lung fibrosis via the midkine signaling pathway. *Am J Respir Crit Care Med* 2015; 192(3): 315–323
  34. Güngör C, Zander H, Effenberger KE, Vashist YK, Kalinina T, Izbicki JR, Yekebas E, Bockhorn M. Notch signaling activated by replication stress-induced expression of midkine drives epithelial-mesenchymal transition and chemoresistance in pancreatic cancer. *Cancer Res* 2011; 71(14): 5009–5019
  35. Zhao G, Nie Y, Lv M, He L, Wang T, Hou Y. ER $\beta$ -mediated estradiol enhances epithelial mesenchymal transition of lung adenocarcinoma through increasing transcription of midkine. *Mol Endocrinol* 2012; 26(8): 1304–1315
  36. Huang Y, Hoque MO, Wu F, Trink B, Sidransky D, Ratovitski EA. Midkine induces epithelial–mesenchymal transition through Notch2/Jak2–Stat3 signaling in human keratinocytes. *Cell Cycle* 2008; 7(11): 1613–1622
  37. Misa K, Tanino Y, Wang X, Nikaido T, Kikuchi M, Sato Y, Togawa R, Tanino M, Tanaka S, Kadomatsu K, Munakata M. Involvement of midkine in the development of pulmonary fibrosis. *Physiol Rep* 2017; 5(16): e13383
  38. Wang QL, Wang H, Zhao SL, Huang YH, Hou YY. Over-expressed and truncated midkines promote proliferation of BGC823 cells *in vitro* and tumor growth *in vivo*. *World J Gastroenterol* 2008; 14(12): 1858–1865
  39. Rajasekaran K, Xiong V, Fong L, Gorski J, Malarkannan S. Functional dichotomy between NKG2D and CD28-mediated costimulation in human CD8<sup>+</sup> T cells. *PLoS One* 2010; 5(9): e12635
  40. Gardner A, Fisher AJ, Richter C, Johnson GE, Moisey EJ, Brodli M, Ward C, Krippner-Heidenreich A, Mann DA, Borthwick LA. The critical role of TAK1 in accentuated epithelial to mesenchymal transition in obliterative bronchiolitis after lung transplantation. *Am J Pathol* 2012; 180(6): 2293–2308
  41. Tian R, Zhu Y, Yao J, Meng X, Wang J, Xie H, Wang R. NLRP3 participates in the regulation of EMT in bleomycin-induced pulmonary fibrosis. *Exp Cell Res* 2017; 357(2): 328–334
  42. Vyas-Read S, Wang W, Kato S, Colvocoresses-Dodds J, Fifadara NH, Gauthier TW, Helms MN, Carlton DP, Brown LA. Hyperoxia induces alveolar epithelial-to-mesenchymal cell transition. *Am J Physiol Lung Cell Mol Physiol* 2014; 306(4): L326–L340
  43. Suzuki N, Shibata Y, Urano T, Murohara T, Muramatsu T, Kadomatsu K. Proteasomal degradation of the nuclear targeting growth factor midkine. *J Biol Chem* 2004; 279(17): 17785–17791
  44. Phan SH. The myofibroblast in pulmonary fibrosis. *Chest* 2002; 122 (6 Suppl): 286S–289S
  45. Zhao H, Wu QQ, Cao LF, Qing HY, Zhang C, Chen YH, Wang H, Liu RY, Xu DX. Melatonin inhibits endoplasmic reticulum stress and epithelial-mesenchymal transition during bleomycin-induced pulmonary fibrosis in mice. *PLoS One* 2014; 9(5): e97266
  46. Marudamuthu AS, Bhandary YP, Shetty SK, Fu J, Sathish V, Prakash Y, Shetty S. Role of the urokinase-fibrinolytic system in epithelial-mesenchymal transition during lung injury. *Am J Pathol* 2015; 185(1): 55–68
  47. Kyung SY, Kim DY, Yoon JY, Son ES, Kim YJ, Park JW, Jeong SH. Sulforaphane attenuates pulmonary fibrosis by inhibiting the epithelial-mesenchymal transition. *BMC Pharmacol Toxicol* 2018; 19(1): 13

48. Kim KK, Kugler MC, Wolters PJ, Robillard L, Galvez MG, Brumwell AN, Sheppard D, Chapman HA. Alveolar epithelial cell mesenchymal transition develops *in vivo* during pulmonary fibrosis and is regulated by the extracellular matrix. *Proc Natl Acad Sci USA* 2006; 103(35): 13180–13185
49. Kalluri R, Neilson EG. Epithelial-mesenchymal transition and its implications for fibrosis. *J Clin Invest* 2003; 112(12): 1776–1784
50. Tanjore H, Xu XC, Polosukhin VV, Degryse AL, Li B, Han W, Sherrill TP, Plieth D, Neilson EG, Blackwell TS, Lawson WE. Contribution of epithelial-derived fibroblasts to bleomycin-induced lung fibrosis. *Am J Respir Crit Care Med* 2009; 180(7): 657–665
51. Kim KK, Wei Y, Szekeres C, Kugler MC, Wolters PJ, Hill ML, Frank JA, Brumwell AN, Wheeler SE, Kreidberg JA, Chapman HA. Epithelial cell  $\alpha 3\beta 1$  integrin links  $\beta$ -catenin and Smad signaling to promote myofibroblast formation and pulmonary fibrosis. *J Clin Invest* 2009; 119(1): 213–224
52. Huang Y, Hoque MO, Wu F, Trink B, Sidransky D, Ratovitski EA. Midkine induces epithelial-mesenchymal transition through Notch2/Jak2–Stat3 signaling in human keratinocytes. *Cell Cycle* 2008; 7(11): 1613–1622
53. Misa K, Tanino Y, Wang X, Nikaido T, Kikuchi M, Sato Y, Togawa R, Tanino M, Tanaka S, Kadomatsu K, Munakata M. Involvement of midkine in the development of pulmonary fibrosis. *Physiol Rep* 2017; 5(16): e13383
54. Liu F, Gomez Garcia AM, Meyskens FL Jr. NADPH oxidase 1 overexpression enhances invasion via matrix metalloproteinase-2 and epithelial-mesenchymal transition in melanoma cells. *J Invest Dermatol* 2012; 132(8): 2033–2041
55. Kesanakurti D, Maddirela D, Banasavadi-Siddegowda YK, Lai TH, Qamri Z, Jacob NK, Sampath D, Mohanam S, Kaur B, Puduvali VK. A novel interaction of PAK4 with PPAR $\gamma$  to regulate Nox1 and radiation-induced epithelial-to-mesenchymal transition in glioma. *Oncogene* 2017; 36(37): 5309–5320
56. Das SJ, Lovicu FJ, Collinson EJ. Nox4 plays a role in TGF- $\beta$ -dependent lens epithelial to mesenchymal transition. *Invest Ophthalmol Vis Sci* 2016; 57(8): 3665–3673
57. Rao YK, Fang SH, Tzeng YM. Evaluation of the anti-inflammatory and anti-proliferation tumoral cells activities of *Antrodia camphorata*, *Cordyceps sinensis*, and *Cinnamomum osmophloeum* bark extracts. *J Ethnopharmacol* 2007; 114(1): 78–85
58. Ko YF, Liao JC, Lee CS, Chiu CY, Martel J, Lin CS, Tseng SF, Ojcius DM, Lu CC, Lai HC, Young JD. Isolation, culture and characterization of *Hirsutella sinensis* mycelium from caterpillar fungus fruiting body. *PLoS One* 2017; 12(1): e0168734
59. Datta A, Kim GA, Taylor JM, Gugino SF, Farrow KN, Schumacker PT, Berkelhamer SK. Mouse lung development and NOX1 induction during hyperoxia are developmentally regulated and mitochondrial ROS dependent. *Am J Physiol Lung Cell Mol Physiol* 2015; 309(4): L369–L377
60. Zanetti F, Giacomello M, Donati Y, Carnesecchi S, Frieden M, Barazzone-Argiroffo C. Nicotine mediates oxidative stress and apoptosis through cross talk between NOX1 and Bcl-2 in lung epithelial cells. *Free Radic Biol Med* 2014; 76: 173–184